Journal of Reproduction and Development, Vol. 66, No 4, 2020

—Original Article—

Repeated hyperstimulation affects the ultrastructure of mouse fallopian tube epithelium

Sevastiani ANTONOULI[1)*], Maria Grazia PALMERINI[1)*], Serena BIANCHI[1)], Gianna ROSSI[1)], Sandra CECCONI[1)], Manuel BELLI[1)], Sara BERNARDI[1)], Mohammad Ali KHALILI[2)], Giuseppe FAMILIARI[3)], Stefania Annarita NOTTOLA[3)] and Guido MACCHIARELLI[1)]

[1)]*Department of Life, Health and Environmental Sciences, University of L'Aquila, 67100 L'Aquila, Italy*
[2)]*Department of Reproductive Biology, Yazd Institute for Reproductive Sciences, Shahid Sadoughi University of Medical Sciences, Yazd, Iran*
[3)]*Department of Anatomy, Histology, Forensic Medicine and Orthopaedics, University of Rome La Sapienza, Rome, Italy*

Abstract. Controlled ovarian hyperstimulation (COH) is routinary used in assisted reproductive technologies (ARTs) to increase the yields of mature oocytes. The possibility that patients with a history of failures or poor-responders may develop side-effects following these treatments is still debated. Epidemiological studies reported controversial results about pregnancy outcome and the risk of developing gynecological cancers. By using a mouse model, here we compared the ultrastructural features of fallopian tubes (FTs) obtained from mice undergoing or not (control, CTR) four (4R) and eight (8R) rounds of gonadotropin stimulation. Although the morphological characteristics of oviductal layers seemed unaffected by repeated treatments, dose-response ultrastructural alterations in the ampulla appeared in the 4R group and even more in the 8R group. The targets were oviductal ciliated (CCs) and non-ciliated (NCCs) cells, which showed damaged mitochondria and glycogen accumulations in the cytoplasm. The drastic reduction of CCs, evident after 4R, was supported by the absence of cilia. After 8R, glycogen granules were significantly reduced and massive degeneration of mitochondria, which appeared swollen and/or vacuolated, occurred in NCCs. Moreover, disintegrated mitochondria were found at the periphery of mitophagic vacuoles with evident signs of cristolysis. The morphometric analysis evidenced a significant increase in the density and frequency of damaged mitochondria after 4R and 8R. The absence of cilia, necessary to sustain oviductal transport of oocytes, spermatozoa and embryos, may originate from either mitochondrial dysfunction or glycogen consumption. These results suggest that repeated COH treatments could induce alterations impairing fertilization and embryo transport toward the uterus.
Key words: Columnar epithelial cells, Controlled ovarian hyperstimulation, Electron microscopy, Fallopian tubes, Mouse
(**J. Reprod. Dev. 66:** 387–397, 2020)

Controlled ovarian hyperstimulation (COH) is routinely used in Assisted Reproductive Technologies (ARTs) to increase the number of retrieved mature oocytes and, therefore, to enhance the success rate of these protocols [1]. However, increased number of treatments (n > 4), especially with gonadotropins, can induce complications in treated patients, including premature progesterone elevation throughout the follicular phase, defective endometrium receptivity, luteal phase insufficiency or severe ovarian hyperstimulation syndrome (OHSS) [2–4]. Although the relationship between hyperstimulation and cancer is still controversial [5, 6], a major risk is that COH-induced supraphysiologic estrogen (E2) levels may promote, with time, the growth of estrogen-sensitive tumors, such as endometrial, ovarian and estrogen receptor-positive breast cancers [7–9].

An interesting question is how fallopian tubes (FTs) could respond to COH. Indeed, during the reproductive cycle, hormonal oscillations impact on the histophysiology of the FTs and, specifically, of the *tunica mucosa* [10, 11]. In mice, the relationship between the number of columnar epithelial ciliated cells and non-ciliated cells - also known as secretory, intercalar or peg cells –changes during the hormonal cycle with the predominance of ciliated cells during the follicular phase and of secretory cells during the luteal phase, even if with individual differences [12]. In this species, E2 stimulates epithelial cell hypertrophy, cilia beat frequency (CBF) and oviductal secretions [13], while progesterone (P) acts on *tunica mucosa* by inducing epithelial cell atrophy, deciliation and decrease of CBF [14, 15]. If P production is altered, a delay in the transportation timing of the ovum or zygotes occurs [16].

In our previous papers, we analyzed oocyte spindle morphology and the content of proteins involved in cell cycle control in ovaries and FTs retrieved from mice treated up to 8 times (8 Rounds, 8R) with a standardized protocol of gonadotropin [17, 18]. Despite after 4R the only modification recorded was an increase in cyclin D1 content in FT, after 8R also p53, phospho-p53, phospho-AKT, GSK3B and OCT3/4 contents were significantly higher than in controls. The

Received: November 14, 2019
Accepted: April 15, 2020
Advanced Epub: April 28, 2020

Correspondence: MG Palmerini (e-mail: mariagrazia.palmerini@univaq.it)
* S Antonouli and MG Palmerini contributed equally to this work.

over-expression of these proteins, all involved in the control of cell cycle progression, and the drastic decrease of oocyte number and spindle quality strongly supported an altered differentiation processes of FT epithelial cells and an impaired ovulation and oocytes spindle organization [17–19].

Physiological/pathological changes of FT epithelium have been found in different species as rat [20], hamster [21], pig [22], goat [23] and horse [24]. Also, the ultrastructural features of mucosa and epithelial cells, such as the presence, distribution, and location of secretory and ciliated cells in the various portions of the human and murine FTs during the hormonal cycle have been described [25, 26]. Interestingly, in mouse FTs the percentage of the ampullar epithelial cells and their proliferation rate were found to be estrus cycle-dependent [26]. Exogenous ovarian steroids, especially E2, accelerate the differentiation and maturation of secretory cells in mouse FTs [27].

However, the effects on FT ultrastructure exerted by COH are, to our knowledge, not yet investigated. Therefore, in the present study, we evaluated the ultrastructure of the ampulla, the third portion of mouse FTs, following 4R and 8R of gonadotropin administration by transmission (TEM) and scanning (SEM) electron microscopy.

Materials and Methods

Animals

Mus musculus Swiss CD1 female adult mice (2–3-month-old; Harlan Italy, Udine, Italy, n = 15) were housed in the animal facility under controlled temperature (21 ± 1°C), with 12:12 h light: dark cycle and free access to food and water. All the experimental procedures and the animals were maintained in accordance with national and international law and policies (European Economic Community Council Directive 86/609, OJ 358, 1 Dec 12, 1987; Italian Legislative Decree 116/92, Gazzetta Ufficiale della Repubblica Italiana n. 40, Feb 18, 1992; National Institutes of Health Guide for the Care and Use of Laboratory Animals, NIH publication no. 85-23, 1985). The Italian Ministry of Health and the local committee (University of L'Aquila) for the animal care and use approved the experimental protocols, in compliance with the accepted veterinary medical practice. Animals were euthanized by cervical dislocation after an inhalant overdose of carbon dioxide (CO_2, 10–30%), followed by cervical dislocation. All efforts were made to minimize animal suffering.

Experimental protocols and hormonal treatments

Animals in which the early luteal phase of the estrous cycle was evaluated by examination of the vagina and vaginal smears (n = 4), and without any hyperstimulation, were used as Control (Ctr). Repetitive cycles of ovarian stimulation were performed according to previous studies [17, 18]. Briefly, mice (ν = 11) were injected i.p. with 5 IU of PMSG (pregnant mare serum gonadotropin) (Folligon, Milano, Italy) and after 48 h with 5 IU of hCG (human chorionic gonadotropin) (Corulon, Milano, Italy). The timing of four to eight repeated rounds (4R, 8R) of stimulation was selected according to [17] and [18]. In particular, the COH protocol (PMSG + hCG) was repeated four times in the mice of 4R group (n = 6) and eight times in those of 8R group (n = 5). All the rounds were performed at intervals of one week between each. After approximately 16 hours from the last hCG injection (in the 4^{th} and 8^{th} week respectively), mice were sacrificed as described above. From each animal, both oviducts were collected, washed in PBS and used for light and electron microscopy analysis.

Light microscopy (LM) and TEM

Left FTs were isolated from their neighboring ovaries, gently washed in phosphate-buffered saline (PBS) solution and immediately fixed in 2.5% glutaraldehyde (Agar Scientific, Stansted, UK)/0.1 M PBS. Fixed samples were maintained at 4°C for at least 48 h until the next preparative for TEM [28–31]. Firstly, FTs from each experimental group (Ctr, 4R, 8R) were cut into small sections to isolate the third portion, i.e. the ampullae. Successively, the pieces were rinsed in PBS, post-fixed with 1% osmium tetroxide (Agar Scientific)/0.1 M PBS and rinsed again in 0.1 M PBS. Samples were then dehydrated in ascending series of ethanol (Carlo Erba Reagenti, Milan, Italy), immersed in propylene oxide (BDH Italia, Milan, Italy) for solvent substitution and embedded in epoxy resin EMbed-812 (Electron Microscopy Sciences, Hatfield, PA, USA). Semithin sections (1 mm thick) were stained with Methylene Blue, examined using a LM (Zeiss Axioskop, Oberkochen, Germany) and photographed using a digital camera (DFC230; Leica, Wetzlar, Germany). Ultrathin sections (60–80 nm) were cut with a diamond knife, on a Reichert-Jung Ultracut E ultramicrotome (Reichert Technologies, Munich, Germany), mounted on copper grids and contrasted with saturated uranyl acetate followed by lead citrate (SIC, Rome, Italy). They were examined and photographed using Zeiss EM10 and Philips TEM CM100 Electron Microscopes operating at 80 kV.

We evaluated the following parameters for the qualitative assessment of the ultrastructural preservation of mouse oviducts: general features; morphology of the *tunica mucosa*, *muscularis* and *serosa*; membrane integrity of the cells; morphology of the nucleus, chromatin, and nuclear envelope; type and quality of organelles and inclusions; configuration of mitochondria; type of granules, vesicles and vacuoles; intercellular projections; microvillus pattern and presence or extent of cilia [32–36].

SEM

Ampullar samples of the right FTs were processed for conventional [37–41] and variable pressure (VPSEM) SEM analysis. For each experimental group (Ctr, 4R, 8R), the isolated oviducts of their neighboring ovaries were fixed in 2.5% glutaraldehyde/0.1 M PBS at 4°C for at least 48 h. Selected sections of ampulla were processed either for conventional or VPSEM preparation. Briefly, fixed samples were washed in 0.1 M PBS, post-fixed in 1% osmium tetroxide (Agar Scientific)/0.1 M PBS, washed again in 0.1 M PBS and dehydrated in ascending ethanol series (Carlo Erba Reagenti). Following critical point drying in a CO_2 atmosphere (Emitech K850; Ashford, Kent, UK), samples processed for conventional SEM and VPSEM analysis were mounted onto aluminum stubs and coated with platinum (4 nm in thickness) (Emitech K550 sputter coater; Ashford). The observations were performed at a low accelerating voltage (5–10 kV) in conventional SEM (S-4000; Hitachi, Tokyo, Japan) and at higher accelerating voltage (15 kV) in VPSEM (SU 3500; Hitachi) [32, 35, 42, 43].

Morphometric analysis

The ImageJ software (http://rsbweb.nih.gov/ij/) was used to measure the numerical density and dimension of normal and damaged mitochondria from columnar epithelial cells (CECs) of the *tunica mucosa* on low-magnification TEM micrographs of Ctr, 4R and 8R groups. The numerical density of mitochondria was expressed as number of organelle per 100 μm^2 of epithelial area [44]. Mitochondria were classified, according to their ultrastructural appearance, in: i) normal, i.e. intact, with round/elongated shape, with electron-dense lamellar cristae; ii) damaged, with either swollen, irregular, or deficient cristae; patchy or degenerated matrix and evident breaks in the wall of mitochondrial membrane. The quantity/plethora of normal and damaged mitochondria per group was also expressed as percentage of total mitochondria numerical density. For each experimental group, at least three sections from three different experiments were selected for the morphometric analysis.

Statistical analysis

Dimension and numerical density of normal and damaged mitochondria were expressed as mean ± standard deviation (SD). Statistical comparisons were performed using one-way ANOVA with Tukey's honest significant difference (HSD) tests for post-hoc analysis (GraphPad InStat; GraphPad Software, La Jolla, USA). Differences in values were considered significant if $P < 0.05$.

Results

Control group

By LM, the *tunica mucosa* of the ampullar region of FTs was folded in many branches projecting into the lumen and constituted by CECs, ciliated (CCs) and non-ciliated (NCCs) (Fig. 1A). Cuboidal cells were also found. CCs showed less intense staining than the secretory NCs. The CECs presented integral nuclei delimited by an evident nuclear membrane. The *tunica muscularis* showed the characteristic orientation of smooth muscle fibers, arranged in two usually well-defined layers (Fig. 1A). In particular, the outer layer showed individual fiber bundles oriented in a longitudinal plane while the inner one was made of circular fibers. The *tunica serosa*, the external most layer, was made of a squamous mesothelium and an underlying subtle rim of connective tissue (Fig. 1A).

The TEM analysis of the FT epithelium showed that nuclei were roundish-to-amoeboid in shape, delimited with a continuous and electron-dense nuclear membrane often indented (Fig. 1B). Inside the nucleus, the chromatin appeared abundant and uniformly distributed or, occasionally, with heterochromatin clustered in clumps or located as marginal patches under the nuclear membrane (Fig. 1B). In the cytoplasm, numerous round and elongated mitochondria with electron-dense lamellar cristae were visible and interspersed with those characterized by an electron-pale content. Mitochondria were often found in association with thin endoplasmic reticulum (ER) tubules and/or networks (Figs. 1B–1D). Highly electron-dense secondary lysosomes and multivesicular bodies were frequently detected (Fig. 1C). Lipid droplets (Fig. 1B) and Golgi apparatus were rarely found scattered throughout the CEC cytoplasm. The cytoplasm also contained moderate electron-dense aggregates of glycogen particles (Fig. 1C, Fig. 1E). Electron-negative vacuoles were rarely seen. CCs appeared electron-lucent with motile cilia protruding into the lumen. They consisted of an evident axoneme of nine peripheral doublet microtubules, surrounding a central complex with two central microtubules and the central sheath (9 + 2 arrangement) (Fig. 1E). Among the cilia, numerous long and thin microvilli were also evident (Figs. 1B–1E). The luminal side of CCs contained the typical cylindric basal bodies, located in rows immediately beneath the cell membrane (Fig. 1E). NCs showed apical protrusions with numerous short and long microvilli, usually continuous; occasionally, areas with rare microvilli were detected (Fig. 1C, Fig. 1D). It was also noticed the presence of dense secretory granules (Fig. 1C, Fig. 1D). Junctional complexes between neighboring epithelial cells were well developed (Fig. 1B). Usually, adjacent epithelial cells were connected by apical *zonulae occludens*, followed by *zonulae adhaerens* (Fig. 1B, Fig. 1D).

4 ROUNDS

After 4R of COH, the *tunica mucosa* of FTs was folded and highly branched, as seen by LM. The epithelium, as in the control group, was made by a single layer of cuboidal or columnar cells, whose round/ovoid nuclei were intensely stained (Fig. 2A). Both the outer and the inner layers of the *tunica muscularis* were visible in transversal sections (Fig. 2A). The *tunica serosa* did not show any difference in respect to controls (Fig. 2A).

The ultrastructural analysis by TEM showed single-layered CECs with round-to-ovoidal nuclei delimited by an uninterrupted electron-dense nuclear membrane. Irregularly shaped nuclei showed a marginal organization of electron-dense heterochromatin, sometimes organized in highly condensed patches, with occasionally dense nucleoli (Figs. 2B–E). In the cytoplasm, round/elongated and electron-dense mitochondria were found together with abundant severely swollen mitochondria, characterized by a pale and marginalized content, degenerated matrix and a few or damaged cristae (Figs. 2B–F). Numerous electron-negative vesicles were observed and, at high magnification, most of them were autophagosomes containing degraded mitochondria (Fig. 2E and *inset*). Prominent intracytoplasmic vacuoles lined by microvilli were occasionally detected, presumably corresponding to intracytoplasmic pouches of the plasma membrane (Fig. 2F). Multivesicular bodies with large vesicles, high electron-dense secondary lysosomes, ER tubular elements, and lipid droplets were also found (Fig. 2B, Fig. 2D). Small elements of the Golgi complex and glycogen accumulations were rarely detected (not shown). Among CECs, intercellular junctions were well preserved and organized as in controls (Fig. 2B, Fig. 2C). The microvillar distribution pattern in NCs did not show evident variations, respect to those seen in the control group. However, areas with rare microvilli were occasionally found (Fig. 2B, Fig. 2C). In the observed sections, CCs were not found.

8 ROUNDS

After 8R, the *tunica mucosa* and *tunica muscularis* did not appear different respect to the previous groups, as seen by LM (Fig. 3A). The nuclei of CECs from the highly folded *tunica mucosa* and the two layers of *tunica muscularis* were detected, as previously described (Fig. 3A). The *tunica serosa*, when visible in section, did not show any difference in respect to the previous groups (Fig. 3A).

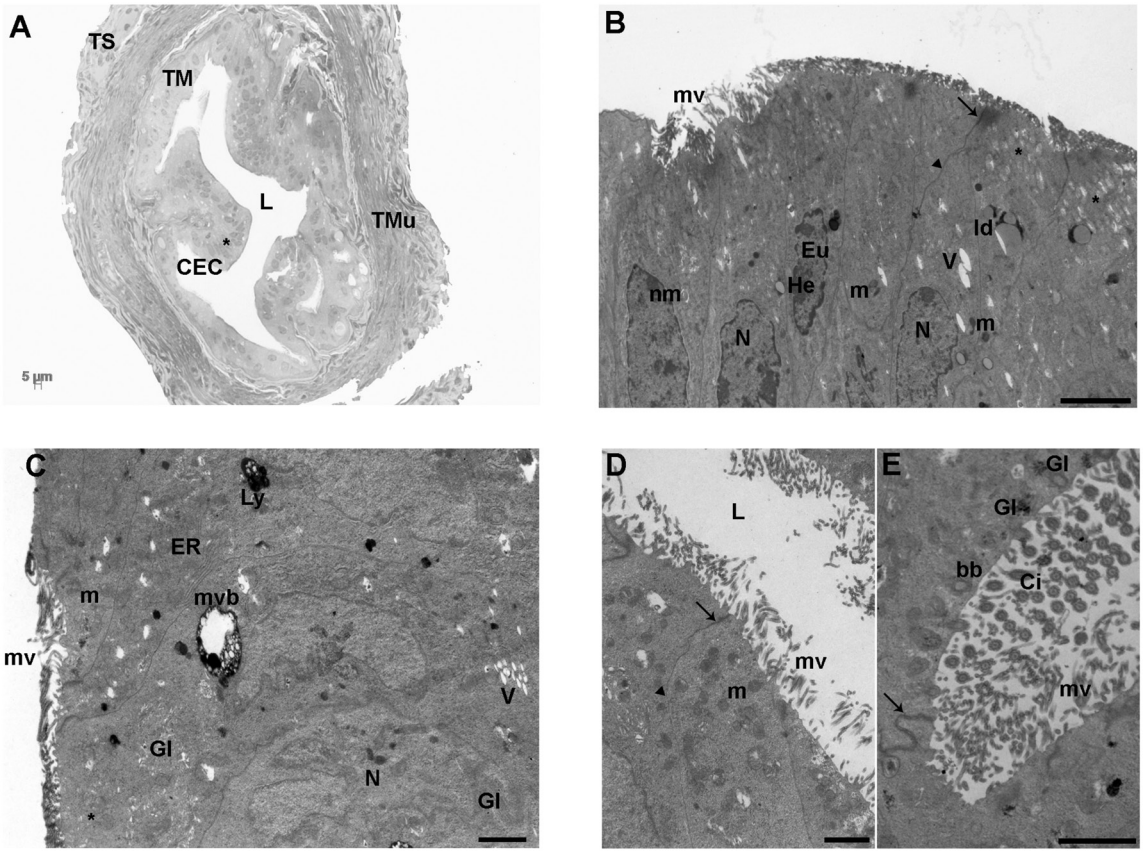

Fig. 1. Control group. A) Representative LM picture of a transversal section of mouse ampulla showing the three layers of *tunica mucosa* (TM), *muscularis* (TMu) and *serosa* (TS). The TM appears regularly folded and characterized by adjacent columnar epithelial cells (CEC) with evident nuclei (*). In the *tunica muscularis* (TMu), the two well-defined outer and inner layers are evident. The former is organized in individual smooth muscle fiber bundles longitudinally oriented while the latter is organized in circular fibers. L: lumen (LM. Mag: 20 ×. Bar: 5 µm). B) Ultrastructure of the columnar epithelium of TM, showing roundish-to-amoeboid shaped nuclei (N) delimited by a continuous nuclear membrane (nm). Heterochromatin (He) was clustered in clumps or located as marginal patches under the nuclear envelope among the dispersed euchromatin (Eu). The cytoplasm contains numerous round or elongated mitochondria (m), with electron-dense lamellar cristae or electron-pale content; lipid droplets (ld), short and long microvilli (mv), a few electron-negative vacuoles (V) and secretory granules with a slightly electron-dense content (asterisks). The junctional complexes between neighboring epithelial cells appear well-formed and constituted from the lumen by *zonulae occludens* (arrow) followed by *zonulae adherens* (arrowhead) [transmission electron microscopy (TEM). Bar: 2 µm]. C) CECs of TM showing a large multivesicular body (mvb), an electron-dense secondary lysosome (Ly), tubular elements of the endoplasmic reticulum (ER), well-defined nuclei (N) and mitochondria (m). V: vacuoles; mv: microvilli; Gl: glycogen granules; asterisk: secretory granules (TEM. Bar: 1 µm). D) The luminal side (L) of TM shows numerous short or long microvilli (mv). m: mitochondria; arrows: zonulae occludens; arrowhead: *zonula adherens* (TEM. Bar: 1 µm). E) High magnification of motile cilia (Ci) showing an evident axoneme of nine peripheral doublet microtubules, surrounding a central complex with two central microtubules and the central sheath (9 + 2 arrangement). Gl: glycogen granule; arrows: *zonula occludens* (TEM. Bar: 2 µm).

TEM analysis showed that the general ultrastructure of nuclei, lipid droplets, ER tubules/networks, Golgi apparatus, secondary lysosomes, multivesicular bodies, microvilli and intercellular connections was similar between 4R and 8R (Figs. 3B–F). Similarly to the 4R group, the most evident and peculiar morphological alterations affected the mitochondria. Mitochondrial damages were observed more frequently respect to 4R. They ranged from a severely swollen appearance up to a disrupted aspect with electron-negative content and partial or complete cristolysis (Fig. 3C). The matrix of swollen mitochondria appeared patchy, and often, the mitochondrial membrane presented evident breaks in the wall (Figs. 3B–D). Mitochondria showing a partly swollen aspect, with some area of still dense matrix, were also found together with a few rounds/elongated normal electron-dense mitochondria with lamellar cristae (Fig. 3B). Mitophagic vacuoles were often close to lysosomes or multivesicular bodies (Fig. 3E). Secretory granules, with an electron-dense homogeneous content, appeared beneath the cell surface facing the lumen in NCs (Fig. 3F). Coated vesicles were occasionally detected as in the 4R group; CCs with cilia projecting into the lumen and glycogen accumulations were not found in the observed sections.

Surface ultrastructural analysis by SEM

Representative micrographs of CECs of *tunica mucosa* from the ampullar region of FTs taken by conventional SEM (Figs. 4A–C) and

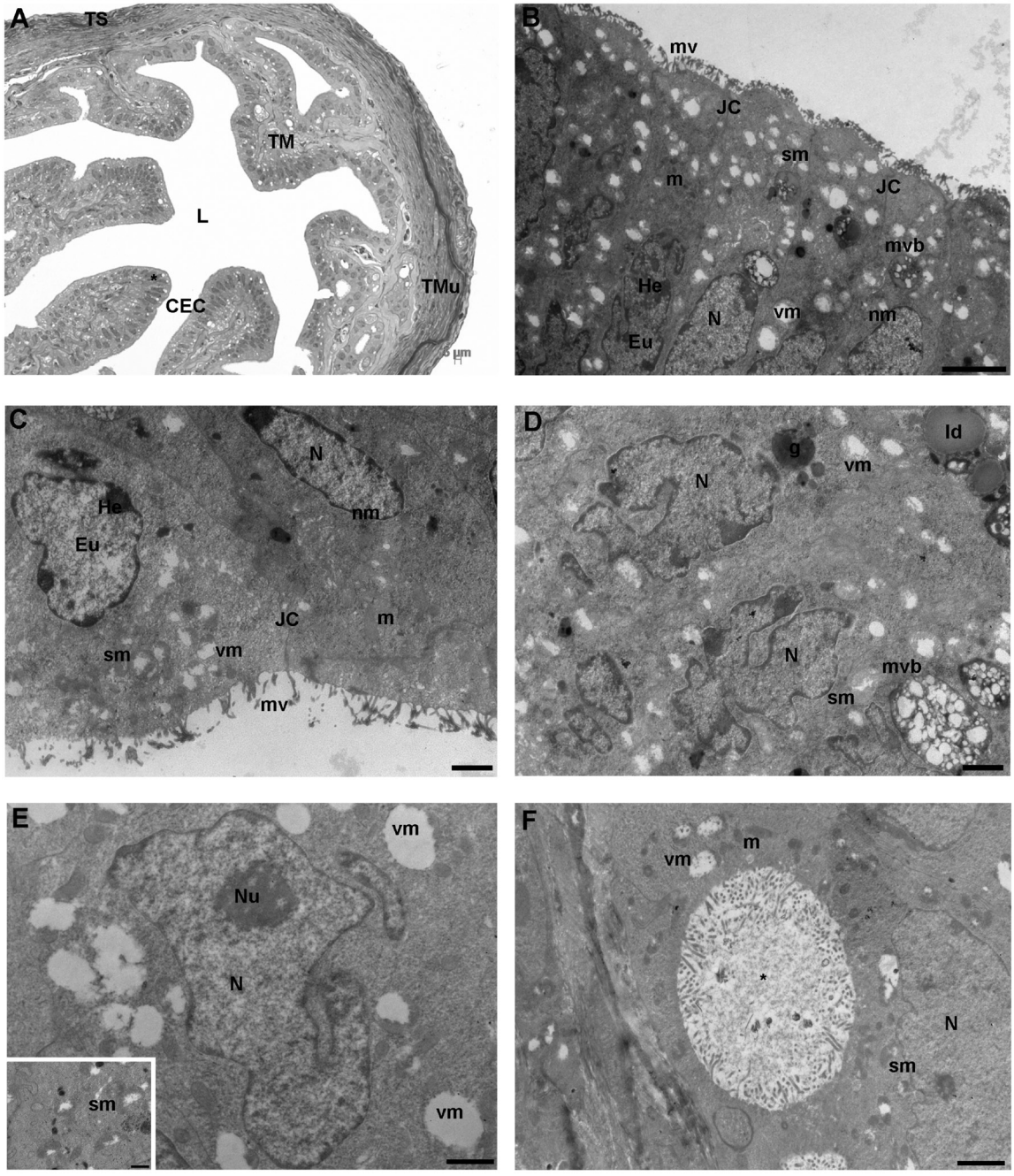

Fig. 2. 4 round (R) group. A) Representative picture of a transversal section of mouse ampulla presenting a highly folded and branched *tunica mucosa* (TM), characterized by columnar epithelial cells (CEC) with intensely stained prominent nuclei (asterisk). The outer and inner layers of *tunica muscularis* (TMu) consist of longitudinal and circular fibers, respectively, from the outer to the inner portion, similarly to the control group. L: lumen (LM. Mag: 20 ×. Bar: 5 μm). B) The surface of *tunica mucosa* shows round-to-ovoidal or irregularly shaped nuclei (N) delimited by an uninterrupted electron-dense nuclear membrane (nm); the chromatin was organized as in control group. The cytoplasmic membrane is folded in a continuous layer of microvilli (mv). The cytoplasm contains multivesicular bodies (mvb), well-defined junctional complexes (JC) and rare round/elongated electron-dense mitochondria (m). Numerous damaged mitochondria with signs of swelling (sm) or vacuolization (vm) are shown. He: heterochromatin; Eu: euchromatin [transmission electron microscopy (TEM). Bar: 2 μm]. C) Magnified micrograph of CECs with two evident nuclei containing patches of heterochromatin (He) clustered under the nuclear membrane (nm). the microvillar coverage (mv) shows numerous interruptions. Eu: euchromatin; nm: nuclear membrane; m: mitochondria; sm: swollen mitochondria; vm: mitophagic vacuoles (TEM. Bar: 1 μm). D) A detail of cytoplasm of an epithelial cell containing strongly indented nuclei, two multivesicular bodies (mvb), an electron-dense granule (g) and lipid droplets (ld). Numerous swelled mitochondria (sm) and mitophagic vacuoles (vm) are visible N: nucleus (TEM. Bar: 1 μm). E) High magnification of a nucleus (N) with a nucleolus (Nu) surrounded by vacuolated mitochondria (vm) with marginalized content (TEM. Bar: 1 μm). *Inset.* Swollen mitochondria (sm) with evident signs of matrix and cristae degeneration (TEM. Bar: 0.6 μm). F) Detail of a big intracytoplasmic vacuole (*) lined by microvilli. N: nucleus; m: mitochondria; sm: swollen mitochondria; vm: mitophagic vacuole (TEM. Bar: 1 μm).

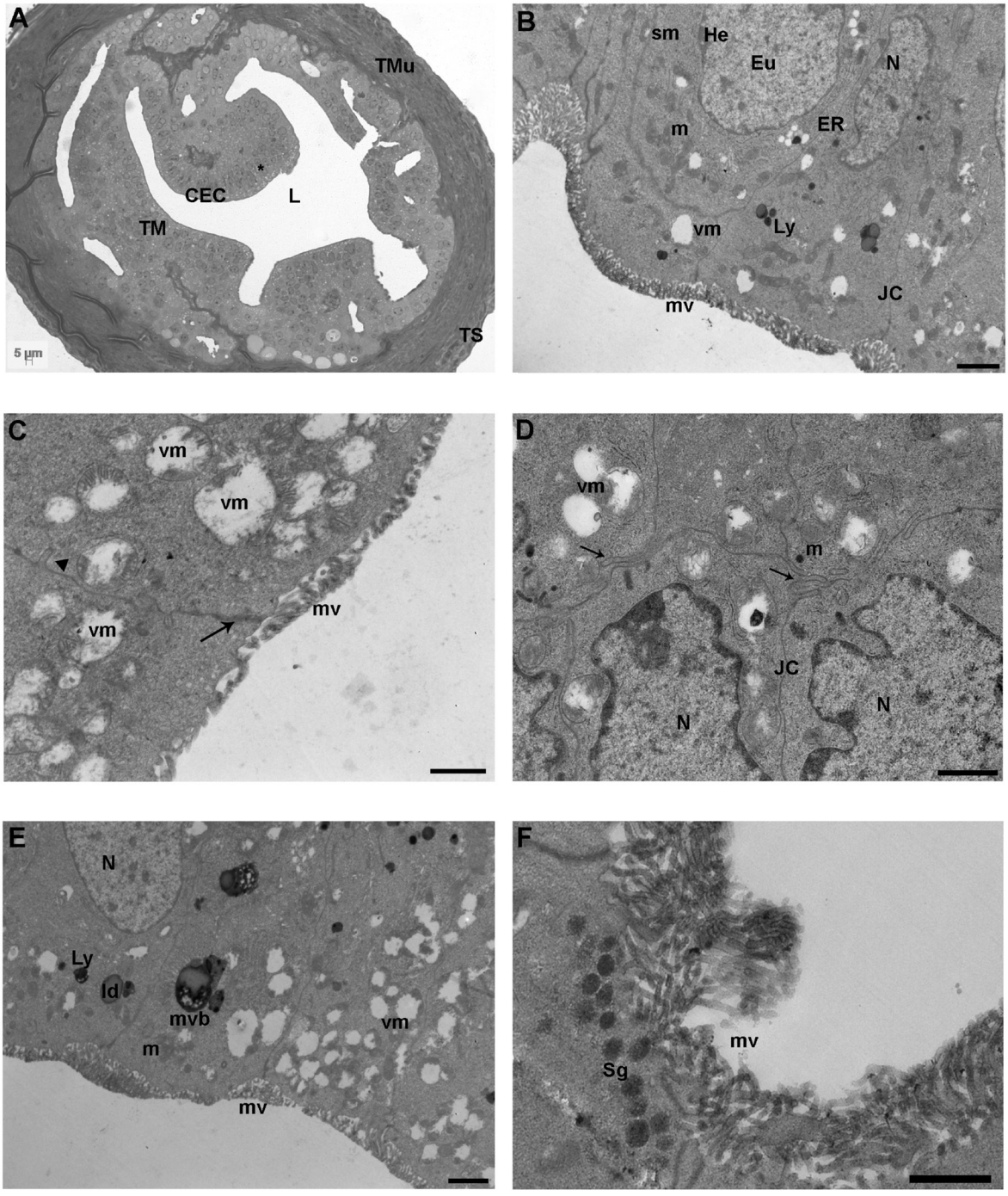

Fig. 3. 8 round (R) group. A) Representative image of a semithin section of the ampullar region of mouse FTs showing the highly folded *tunica mucosa* (TM) with big nuclei (asterisk) and the well-defined two layers of *tunica muscularis* (TMu) and the *tunica serosa* (TS). CECs: columnar epithelial cells, L: lumen (LM. Mag: 20 ×. Bar: 5 µm). B) Micrograph of the *tunica mucosa* showing nuclei (N), round/elongated electron-dense mitochondria (m), endoplasmic reticulum (ER) tubules/networks, secondary lysosomes (Ly), microvilli (mv) and junctional complexes (JC). Eu: euchromatin; He: heterochromatin, sm: swollen mitochondria; vm: vacuolated mitochondria [transmission electron microscopy (TEM). Bar: 1 µm]. C) Detail of damaged mitochondria showing numerous mitophagic vacuoles (vm) characterized by partial or complete cristolysis and peripheric accumulation of the mitochondrial remains. mv: microvilli; arrow: *zonula occludens*; arrowhead: *zonulae adherens* (TEM. Bar: 0.8 µm). D) Epithelial cells showing interdigitated cell contacts (arrows). The cytoplasm contains irregularly shaped nuclei (N) and numerous vacuolated mitochondria (vm). JC: junctional complexes (TEM. Bar: 1 µm). E) Cytoplasmic content of columnar epithelial cells showing numerous mitophagic vacuoles (vm) in proximity to multivesicular bodies (mvb) and lysosomes (Ly). ld: lipid droplet; mv: microvilli; m: mitochondria; N: nucleus (TEM. Bar: 1 µm). F) High magnification of non-ciliated cells rich in electron-dense secretory granules (Sg) with homogeneous content and numerous long and thin microvilli (TEM. Bar: 1 µm).

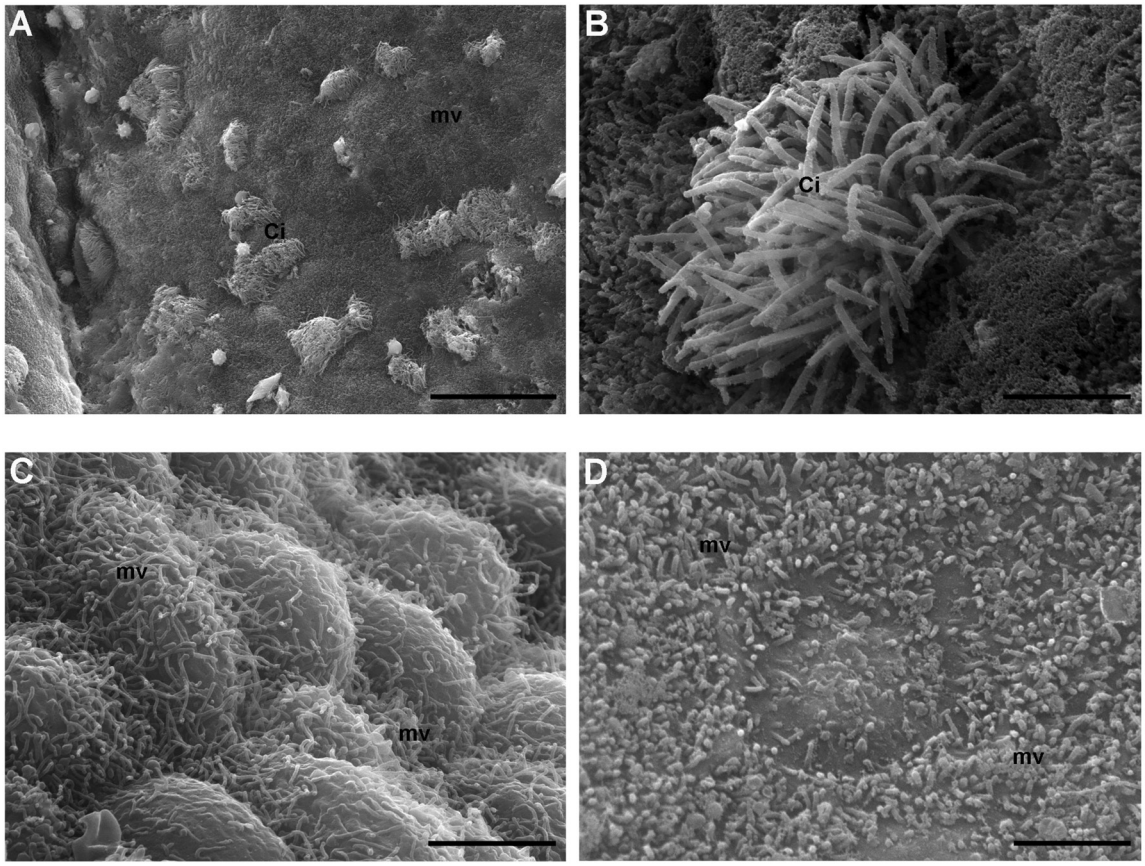

Fig. 4. Surface analysis by scanning electron microscopy (SEM). A–B) Control group. A) Numerous tufts of cilia (Ci) surrounded by short microvilli (mv) protrude into the lumen of the ampullar epithelium (SEM. Bar: 30 μm). B) High magnification of a well-preserved tuft of cilia (Ci) (SEM. Bar: 3 μm). C–D) 4 round (R) group. C) Numerous, long and homogenously distributed microvilli (mv) protrude from the globoid surface of epithelial cells (SEM. Bar: 3 μm). D) Detail of a heterogeneous carpet of short microvilli (mv) (SEM. Bar: 2.5 μm).

VPSEM (Fig. 4D) were selected. A panoramic micrograph showed tufts of cilia nonuniformly distributed in the surface of CCs, protruding into the lumen and surrounded by short microvillar projections of NCs (Fig. 4A, control group). At higher magnification, a single tuft of cilia appeared well preserved (Fig. 4B, control group). Numerous microvilli densely covered the NCs surface. They were long and homogeneous (Fig. 4C, 4R group) or short and not homogeneously distributed (Fig. 4D, 4R group).

Morphometric analysis

Morphometric analysis revealed that the dimension (expressed as mean ± SD) of normal mitochondria per 100 μm^2 was 0.444 ± 0.096 μm in Ctr, 0.415 ± 0.060 μm in 4R and 0.472 ± 0.086 μm in 8R, without significant variations among groups ($P > 0.05$) (Table 1). When dimension was measured in damaged mitochondria, we found a significant increase after 4R (0.553 ± 0.118 μm *vs.* 0.659 ± 0.099 μm; $P < 0.05$) and 8R (0.553 ± 0.118 μm *vs.* 0.817 ± 0.179 μm; $P < 0.001$). This increase was significant also between treated groups (0.659 ± 0.099 μm *vs.* 0.817 ± 0.179 μm, 4R *vs.* 8R respectively; $P < 0.001$) (Table 1).

The numerical density of normal mitochondria dramatically decreased after 4R and 8R, respect to Ctr group (5.3 ± 0.5 and 9.6 ± 4.1 *vs.* 40 ± 12.1, respectively; $P < 0.01$), with no significant variation among treated groups ($P > 0.05$) (Table 1).

Concomitantly, the density of damaged mitochondria significantly increased after 4R, respect to controls (57.6 ± 7.3 *vs.* 22.3 ± 2.3, respectively; $P < 0.01$); however, after 8R the increase was not significant respect to controls (33 ± 7.8 *vs.* 22.3 ± 2.3, respectively; $P > 0.05$) (Table 1).

Quantification of the frequency of damaged mitochondria among groups revealed that their percentage significantly increased after 4R, by reaching the highest values, and less after 8R (36.665 ± 7.629%, 91.45 ± 1.41% , 78.103 ± 4.405%, CTR *vs.* 4R *vs.* 8R, respectively; $P < 0.05$) (Table 1).

Discussion

Gonadotropins are used for COH but their effects after repeated cycles of hyperstimulation on the ampullar epithelium of FTs have not yet investigated from an ultrastructural point of view. We found that, after 4R and 8R, the *tunicae mucosa* and *muscularis* of mouse FTs appeared well-preserved by LM with no evident signs of morphologi-

Table 1. Morphometric analysis

Mitochondria	Normal			Damaged		
	CTR	4R	8R	CTR	4R	8R
Dimension (μm)	0.444 ± 0.096	0.415 ± 0.060	0.472 ± 0.086	0.553 ± 0.118 [a]	0.659 ± 0.099 [b]	0.817 ± 0.179 [c]
Numerical density (N)	40 ± 12.1 [a]	5.3 ± 0.5 [b]	9.6 ± 4.1 [b]	22.3 ± 2.3 [a]	57.6 ± 7.3 [b]	33 ± 7.8 [a]
Percentage (%)	63.335 ± 7.629 [a]	8.550 ± 1.410 [b]	21.897 ± 4.405 [c]	36.665 ± 7.629 [a]	91.450 ± 1.410 [b]	78.103 ± 4.405 [c]

Dimension (μm), numerical density (N) and percentage (%) of normal and damaged mitochondria from columnar epithelial cells of mouse fallopian tube from control (CTR) and after four (4R) and eight (8R) rounds of repeated controlled ovarian hyperstimulation (COH). The morphometric analysis was performed on a 100 μm^2 epithelial area in low-magnification TEM micrographs, from at least three sections from three different experiments per group. Approximately, 40 mitochondria were measured per each experimental group (9–11 mitochondria/animal for control group (n = 4 animals); 6–8 mitochondria/animal for 4R (n = 6 animals); 8–10 mitochondria/animal for 8R (n = 5 animals). Values of each group were expressed as mean ± SD. The percentages of normal or damaged mitochondrial frequency were calculated over the total numerical density. Different superscripts indicate significant differences among the groups of normal or damaged mitochondria ($P < 0.05$). TEM, transmission electron microscopy.

cal alterations, as in other mammals [45, 46]. The ultrastructural analysis of CECs by TEM showed, in all groups, the presence of well-preserved nuclei and cell junctions, lipid droplets, ER tubules/networks, Golgi apparatuses, secondary lysosomes, multivesicular bodies and microvilli, in accordance with the literature describing the physiological morphology of oviducts [23, 24, 27]. However, electron microscopy evidenced specific changes affecting mitochondria and cilia of the CECs of the mucosa layer, especially after 8R.

Literature data show that repeated rounds of hyperstimulation may affect at a different extent the female reproductive tracts by inducing a decrease in the pregnancy rates from 25.2% to 17.8% after the 4R, and up to 11.2% after more than 12R [47]. This can be accounted for significant changes in oocyte and follicular quality, as well as for the reduced developmental potential of embryos [17, 19, 48, 49]. In particular, after 4R there were observed a decrease in the percentage of mouse oocytes with a uniform distribution of mitochondria, an increase in the aggregation of the Golgi apparatus and endoplasmic reticulum, and the induction of spindle disruption [49]. However, in a recent study on women stimulated by a standard antagonist protocol, no adverse effects were found after repeated cycles of COH. At 3R or more the number of mature oocytes, zygotes and clinical pregnancy rates were even higher than those obtained by 2R or less [50]. These contrasting results could be accounted for the milder stimulation used and for a different specie-specific sensitivity that deserves to be better addresses.

Repeated cycles of COH were also connected to oxidative stress. In fact, while ROS production augmented after 4R of COH, the *Oct4* transcripts started to decrease [49]. This is in agreement with our previous data, showing a progressive reduction of the protein OCT3/4 from 4 to 8R in mouse [18]. Moreover, oxidative damages were also detected in mouse ovaries. The oxidative damage, including an increased content of 8-OH-dG, lipid peroxides and protein carbonyls, positively correlated with the number of COH cycles [51]; it induced mitochondrial abnormalities and a decrease in antioxidants compatible with ovarian aging [52]. The effects of COH were determined also in mouse cumulus cells, where the mtDNA copy number decreased as the number of stimulation increased, together with altered DNA methylation in nuclear-encoded DNA polymerase gamma A (PolgA] and consequent changes in PolgA expression [53]. Moreover, mRNA expression levels of cytochrome b (CYTB), cytochrome c oxidase subunit 1 (COX1), NADH dehydrogenase subunit (ND4), and NADH dehydrogenase subunit 2 (ND2), all encoded by mtDNA, were altered following repeated superovulation in cumulus cells [53]. Detrimental effects of repeated cycles of COH on mitochondria were seen by the reduction of ATP production on GV-stage mouse oocytes matured *in vitro* after four rounds [54].

These adverse effects on the mitochondrial function after superovulation in oocytes, cumulus cells and embryos [44, 48, 49], prompted us to focus on the ultrastructure of mitochondria dispersed in the columnar epithelial cells of FTs. Interestingly, it was found the presence of numerous swelled or even disrupted elements, most of them undergoing to phenomena of mitophagy, evident already after 4 repeated cycles, in agreement to a previous study in rabbit oviducts after hCG injection [55]. These ultrastructural alterations of CEC mitochondria due to COH, in agreement with the above reported findings, can be probably responsible for a hampered energetic support of the oviductal epithelium [56, 57]. Moreover, the presence of reduced storage of glycogens after repeated cycles of COH, respect to controls, can further sustain the hypothesized energetic imbalance at a time where it is expected the fertilized egg to be in the FTs and in need of the proper enzymes and nutrients for growth and survival [58–60].

Reactive oxigen species (ROS) are present in the FT fluids [61]. Raised levels of ROS are responsible for aberrations in the tubal environment which result in infertility [62]. We could, therefore, speculate that repeated cycles of COH in FTs could alter hormonal imbalance, inducing stressful condition with the increase of ROS and the reduction of endogenous antioxidants. ROS, as the nitric oxide (NO), have a relaxing effect on the tubal smooth musculature at physiological concentrations but displayed a cytotoxic action when their levels increase [62]. Some isoform of the NO synthase (NOS) is upregulated by hormones and gonadotropins (LH/hCG), thus increasing NO production [63]; this could probably occur after repeated cycles of COH. Furthermore, the mitochondrial manganese superoxide dismutase (Mn-SOD) of epithelial cells is involved in mitigating oxygen toxicity to ovulated oocyted and developing embryos in the FT. Its reduction induces a redox imbalance and subsequent mitochondrial damage, as evidenced by swallowing, vacuolization or barely visible cristae found here and by others [61].

The morphometric analysis evidenced that, after 4R onwards of

COH, there was a significant increase in the frequency and density of damaged mitochondria from the oviductal epithelium, thus strenghtening the ultrastructural observations described [55–57]. The slight improvement observed in terms of density and frequency of damaged mitochondria at 8R, respect to 4R, could be probably due to cytoplasmic remodeling mechanisms activated by the oxidative damage, that may establish domains of autonomous regulation of mitochondrial function and activity, as previously reported in mammalian oocytes and embryos [44, 64].

The mitochondrial dysfunction here observed may, probably, be connected to the absence of ciliated epithelium in the sections observed, as the fibrils' tips during ciliogenesis are laterally connected to mitochondria [65]. Malfunction of the ciliary beat impairs the laminar fluid flow above the FT epithelia, thus likely reducing the clearance of oxidative stress caused by follicular fluid after ovulation [66].

In mouse oviducts, CCs can be rise from NCs under the direction of ovarian steroids [67, 68]. As recently seen in bovine, at least seven types of cells at different translational/transcriptional states of ciliogenesis are present in the oviductal epithelium, and their numbers are regulated by the estrous cycle [69]. This might provide the optimal environment for gamete transport, fertilization and embryo development [69]. The fine tuning of the histoarchitecture of FTs could be particularly sensitive to excessive estrogens induced by COH. After mild stimulation, an increased proliferation was, in fact, observed within the tubal epithelium, with pseudostratification of the epithelial cells and loss of their ciliated border [70]. Increased proliferation and multilayering of the tubal epithelium with the appearance of a micropapillary pattern were frequently observed at higher doses of gonadotropins [70].

FT epithelial cells expressed both estrogen and progesterone receptors, that were down-regulated by treatment with exogenous steroids [70, 71]. However, while membrane steroid-binding proteins (as membrane progestin receptors) are exclusively expressed in CCs of mice and women –to probably control the beating of the cilia or receptor expression via feedback systems [71]– the nuclear Progesteron Receptor (PGR) is immunolocalized also in smooth muscle cells [72]. Here, high levels of progesterone or progestagens promote in the luteal phase relaxation of the sphincter in the isthmus, allowing cilia to transport the pre-embryo into the uterine cavity. Differently, the endogenous rise of estradiol (E2) during the periovulatory period activates contractions of the myosalpinx, aiding the transport of spermatozoa [73].

Gonadotropin receptors (FSHR and LHR) are also expressed in FTs and regulated by ovarian steroids [74]. It is noteworthy that hyperstimulation with FSH downregulated FSHR present in the blood and lympatic vessels of the *tunica* mucosa as well as in the smooth muscle cells, thus affecting angiogenesis, vasculogenesis and oviductal contractions. High doses of eCG/hCG induced a reduction in the protein levels of LHR in the oviductal ampulla with a strong impact on ampullary physiology and function, as glycoprotein syntesis and secretion [75].

The findings obtained from this study may corroborate to the harmful side-effects of the ovarian hyperstimulation in regard to the maintenance of cellular integrity and strengthen the aspect that increased rounds can contribute to the risk of developing gynecological cancers [5, 76]. Endometrial biopsies retrieved from cycling IVF patients, with at least three repeated IVF cycles with no pregnancy, revealed a lower expression of the tumor suppressor p27 and a higher expression of its ligase S-phase kinase-interacting protein-2 (Skp2), compared to non-stimulated normal cycling women [77]. Moreover, in the 25% of patients of the study group, Skp2 expression reached concentrations demonstrated in endometrial carcinoma. These findings suggested that repeated hormone stimulation cycles may disrupt endometrial physiology, potentially towards abnormal proliferation [77]. In fact, it has been found that gonadotropin stimulation could produce tubal and ovarian histopathologic abnormalities with a dose-effect [78]. Moreover, the oviducts were reported to be the origin of OC as the high-grade intraepithelial serous carcinoma and ovarian carcinosarcoma [79, 80], thus making the tubal ligation and hysterectomy methods of choice in reducing the possibility for OC development [81, 82].

In conclusion, the ultrastructural alterations found in mitochondria and ciliar coverage of the mouse FT epithelium after repeated rounds of hyperstimulation, further demonstrate that COH has a detrimental impact on CECs morphology. Due to the role of FTs in ensuring fertilization and the subsequent transport of the embryo in the uterus, ultrastructural alterations here described may also contribute to infertility.

Conflict of interests: The authors declare that they have no competing interests.

Acknowledgments

The authors thank Mr Ezio Battaglione, Laboratory for Electron Microscopy "Pietro M. Motta", Rome, and Miss Aurora Navicella, Laboratory of Biotechnologies of Reproduction, University of L'Aquila. Funds for this study were provided by Departmental grants from the Dept. of Life, Health and Environmental Sciences, University of L'Aquila (RIA, Prof Guido Macchiarelli and Prof Sandra Cecconi) and the Department of Anatomy, Histology, Forensic Medicine and Orthopaedics, La Sapienza University of Rome (University grants, Prof. Stefania Annarita Nottola).

References

1. **Maher JY, Christianson MS.** Controlled ovarian stimulation and triggers in in vitro fertilization: protocol personalization key to optimize outcomes. *Minerva Endocrinol* 2018; **43**: 37–49. [Medline]
2. **Fauser BC, Devroey P.** Reproductive biology and IVF: ovarian stimulation and luteal phase consequences. *Trends Endocrinol Metab* 2003; **14**: 236–242. [Medline] [CrossRef]
3. **El Tokhy O, Kopeika J, El-Toukhy T.** An update on the prevention of ovarian hyperstimulation syndrome. *Womens Health (Lond)* 2016; **12**: 496–503. [Medline] [CrossRef]
4. **Adda-Herzog E, Poulain M, de Ziegler D, Ayoubi JM, Fanchin R.** Premature progesterone elevation in controlled ovarian stimulation: to make a long story short. *Fertil Steril* 2018; **109**: 563–570. [Medline] [CrossRef]
5. **Kroener L, Dumesic D, Al-Safi Z.** Use of fertility medications and cancer risk: a review and update. *Curr Opin Obstet Gynecol* 2017; **29**: 195–201. [Medline] [CrossRef]
6. **Del Pup L, Peccatori FA, Levi-Setti PE, Codacci-Pisanelli G, Patrizio P.** Risk of cancer after assisted reproduction: a review of the available evidences and guidance to fertility counselors. *Eur Rev Med Pharmacol Sci* 2018; **22**: 8042–8059. [Medline]
7. **Rizzuto I, Behrens RF, Smith LA.** Risk of ovarian cancer in women treated with ovarian stimulating drugs for infertility. *Cochrane Database Syst Rev* 2019; **6**: CD008215. [Medline]
8. **Cakmak H, Rosen MP.** Ovarian stimulation in cancer patients. *Fertil Steril* 2013; **99**:

1476–1484. [Medline] [CrossRef]

9. **Diergaarde B, Kurta ML.** Use of fertility drugs and risk of ovarian cancer. *Curr Opin Obstet Gynecol* 2014; **26**: 125–129. [Medline] [CrossRef]
10. **Verhage HG, Mavrogianis PA, Boice ML, Li W, Fazleabas AT.** Oviductal epithelium of the baboon: hormonal control and the immuno-gold localization of oviduct-specific glycoproteins. *Am J Anat* 1990; **187**: 81–90. [Medline] [CrossRef]
11. **Wessel T, Schuchter U, Walt H.** Ciliary motility in bovine oviducts for sensing rapid non-genomic reactions upon exposure to progesterone. *Horm Metab Res* 2004; **36**: 136–141. [Medline] [CrossRef]
12. **Carretero A, Ruberte J, Navarro M.** Female genital organs. *In*: Ruberte J, Carretero A, Navarro M (eds.), Morphological Mouse Phenotyping: Anatomy, Histology and Imaging, 1st ed., Academic Press; 2017: 227–252.
13. **Lyons RA, Saridogan E, Djahanbakhch O.** The reproductive significance of human Fallopian tube cilia. *Hum Reprod Update* 2006; **12**: 363–372. [Medline] [CrossRef]
14. **Paltieli Y, Eibschitz I, Ziskind G, Ohel G, Silbermann M, Weichselbaum A.** High progesterone levels and ciliary dysfunction—a possible cause of ectopic pregnancy. *J Assist Reprod Genet* 2000; **17**: 103–106. [Medline] [CrossRef]
15. **Winuthayanon W, Hewitt SC, Korach KS.** Uterine epithelial cell estrogen receptor alpha-dependent and -independent genomic profiles that underlie estrogen responses in mice. *Biol Reprod* 2014; **91**: 110. [Medline] [CrossRef]
16. **Zhao W, Zhu Q, Yan M, Li C, Yuan J, Qin G, Zhang J.** Levonorgestrel decreases cilia beat frequency of human fallopian tubes and rat oviducts without changing morphological structure. *Clin Exp Pharmacol Physiol* 2015; **42**: 171–178. [Medline] [CrossRef]
17. **Di Luigi G, Rossi G, Castellucci A, Leocata P, Carta G, Canipari R, Nottola SA, Cecconi S.** Repeated ovarian stimulation does not affect the expression level of proteins involved in cell cycle control in mouse ovaries and fallopian tubes. *J Assist Reprod Genet* 2014; **31**: 717–724. [Medline]
18. **Di Nisio V, Rossi G, Palmerini MG, Macchiarelli G, Tiboni GM, Cecconi S.** Increased rounds of gonadotropin stimulation have side effects on mouse fallopian tubes and oocytes. *Reproduction* 2018; **155**: 245–250. [Medline] [CrossRef]
19. **Van Blerkom J, Davis P.** Differential effects of repeated ovarian stimulation on cytoplasmic and spindle organization in metaphase II mouse oocytes matured in vivo and in vitro. *Hum Reprod* 2001; **16**: 757–764. [Medline] [CrossRef]
20. **Yang J, Chi C, Liu Z, Yang G, Shen ZJ, Yang XJ.** Ultrastructure damage of oviduct telocytes in rat model of acute salpingitis. *J Cell Mol Med* 2015; **19**: 1720–1728. [Medline] [CrossRef]
21. **El-Mestrah M, Kan FW.** Ultrastructural and ultracytochemical features of secretory granules in the ampullary epithelium of the hamster oviduct. *Anat Rec* 1999; **255**: 227–239. [Medline] [CrossRef]
22. **Katarzyna SM, Wiesław B, Anna R.** The tunica mucosa of the oviduct in case of ovarian cysts presence in sows. *Folia Histochem Cytobiol* 2010; **48**: 148–156. [Medline] [CrossRef]
23. **Sharma RK, Singh R, Bhardwaj JK.** Scanning and transmission electron microscopic analysis of ampullary segment of oviduct during estrous cycle in caprines. *Scanning* 2015; **37**: 36–41. [Medline] [CrossRef]
24. **Desantis S, Zizza S, Accogli G, Acone F, Rossi R, Resta L.** Morphometric and ultrastructural features of the mare oviduct epithelium during oestrus. *Theriogenology* 2011; **75**: 671–678. [Medline] [CrossRef]
25. **Barberini F, Makabe S, Correr S, Luzi A, Motta PM.** An ultrastructural study of epithelium differentiation in the human fetal fallopian tube. *Acta Anat (Basel)* 1994; **151**: 207–219. [Medline] [CrossRef]
26. **Morita M, Miyamoto H, Sugimoto M, Sugimoto N, Manabe N.** Alterations in cell proliferation and morphology of ampullar epithelium of the mouse oviduct during the estrous cycle. *J Reprod Dev* 1997; **43**: 235–241. [CrossRef]
27. **Lauschova I.** Secretory cells and morphological manifestation of secretion in the mouse oviduct. *Scr Med (Brno)* 2003; **76**: 203–214.
28. **Palmerini MG, Nottola SA, Leoni GG, Succu S, Borshi X, Berlinguer F, Naitana S, Bekmukhambetov Y, Macchiarelli G.** In vitro maturation is slowed in prepubertal lamb oocytes: ultrastructural evidences. *Reprod Biol Endocrinol* 2014; **12**: 115. [Medline] [CrossRef]
29. **Leoni GG, Palmerini MG, Satta V, Succu S, Pasciu V, Zinellu A, Carru C, Macchiarelli G, Nottola SA, Naitana S, Berlinguer F.** Differences in the kinetic of the first meiotic division and in active mitochondrial distribution between prepubertal and adult oocytes mirror differences in their developmental competence in a sheep model. *PLoS One* 2015; **10**: e0124911. [Medline] [CrossRef]
30. **Coticchio G, Dal Canto M, Fadini R, Mignini Renzini M, Guglielmo MC, Miglietta S, Palmerini MG, Macchiarelli G, Nottola SA.** Ultrastructure of human oocytes after in vitro maturation. *Mol Hum Reprod* 2016; **22**: 110–118. [Medline] [CrossRef]
31. **Khalili MA, Shahedi A, Ashourzadeh S, Nottola SA, Macchiarelli G, Palmerini MG.** Vitrification of human immature oocytes before and after in vitro maturation: a review. *J Assist Reprod Genet* 2017; **34**: 1413–1426. [Medline] [CrossRef]
32. **Nottola SA, Cecconi S, Bianchi S, Motta C, Rossi G, Continenza MA, Macchiarelli G.** Ultrastructure of isolated mouse ovarian follicles cultured in vitro. *Reprod Biol Endocrinol* 2011; **9**: 3. [Medline] [CrossRef]
33. **Bianchi S, Macchiarelli G, Micara G, Linari A, Boninsegna C, Aragona C, Rossi G, Cecconi S, Nottola SA.** Ultrastructural markers of quality are impaired in human metaphase II aged oocytes: a comparison between reproductive and in vitro aging. *J Assist Reprod Genet* 2015; **32**: 1343–1358. [Medline] [CrossRef]
34. **Palmerini MG, Zhurabekova G, Balmagambetova A, Nottola SA, Miglietta S, Belli M, Bianchi S, Cecconi S, Di Nisio V, Familiari G, Macchiarelli G.** The pesticide Lindane induces dose-dependent damage to granulosa cells in an in vitro culture. *Reprod Biol* 2017; **17**: 349–356. [Medline] [CrossRef]
35. **Palmerini MG, Belli M, Nottola SA, Miglietta S, Bianchi S, Bernardi S, Antonouli S, Cecconi S, Familiari G, Macchiarelli G.** Mancozeb impairs the ultrastructure of mouse granulosa cells in a dose-dependent manner. *J Reprod Dev* 2018; **64**: 75–82. [Medline] [CrossRef]
36. **Taghizabet N, Khalili MA, Anbari F, Agha-Rahimi A, Nottola SA, Macchiarelli G, Palmerini MG.** Human cumulus cell sensitivity to vitrification, an ultrastructural study. *Zygote* 2018; **26**: 224–231. [Medline] [CrossRef]
37. **Martelli A, Palmerini MG, Russo V, Rinaldi C, Bernabò N, Di Giacinto O, Berardinelli P, Nottola SA, Macchiarelli G, Barboni B.** Blood vessel remodeling in pig ovarian follicles during the periovulatory period: an immunohistochemistry and SEM-corrosion casting study. *Reprod Biol Endocrinol* 2009; **7**: 72. [Medline] [CrossRef]
38. **Macchiarelli G, Nottola SA, Palmerini MG, Bianchi S, Maione M, Lorenzo C, Stifano G, Di Marco E, Correr S.** Morphological expression of angiogenesis in the mammalian ovary as seen by SEM of corrosion casts. *Ital J Anat Embryol* 2010; **115**: 109–114. [Medline]
39. **Macchiarelli G, Palmerini MG, Nottola SA, Cecconi S, Tanemura K, Sato E.** Restoration of corpus luteum angiogenesis in immature hypothyroid rdw rats after thyroxine treatment: morphologic and molecular evidence. *Theriogenology* 2013; **79**: 116–126. [Medline] [CrossRef]
40. **Palmerini MG, Nottola SA, Tunjung WA, Kadowaki A, Bianchi S, Cecconi S, Sato E, Macchiarelli G.** EGF-FSH supplementation reduces apoptosis of pig granulosa cells in co-culture with cumulus-oocyte complexes. *Biochem Biophys Res Commun* 2016; **481**: 159–164. [Medline] [CrossRef]
41. **Bernardi S, Bianchi S, Botticelli G, Rastelli E, Tomei AR, Palmerini MG, Continenza MA, Macchiarelli G.** Scanning electron microscopy and microbiological approaches for the evaluation of salivary microorganisms behaviour on anatase titanium surfaces: In vitro study. *Morphologie* 2018; **102**: 1–6. [Medline] [CrossRef]
42. **Nottola SA, Makabe S, Stallone T, Familiari G, Correr S, Macchiarelli G.** Surface morphology of the zona pellucida surrounding human blastocysts obtained after in vitro fertilization. *Arch Histol Cytol* 2005; **68**: 133–141. [Medline] [CrossRef]
43. **Giusti I, Bianchi S, Nottola SA, Macchiarelli G, Dolo V.** Clinical electron microscopy in the study of human ovarian tissues. *EMBJ* 2019; **14**: 145–151.
44. **Belli M, Zhang L, Liu X, Donjacour A, Ruggeri E, Palmerini MG, Nottola SA, Macchiarelli G, Rinaudo P.** Oxygen concentration alters mitochondrial structure and function in in vitro fertilized preimplantation mouse embryos. *Hum Reprod* 2019; **34**: 601–611. [Medline] [CrossRef]
45. **Abe H, Hoshi H.** Morphometric and ultrastructural changes in ciliated cells of the oviductal epithelium in prolific Chinese Meishan and Large White pigs during the oestrous cycle. *Reprod Domest Anim* 2008; **43**: 66–73. [Medline]
46. **Tienthai P, Sajjarengpong K, Techakumphu M.** Light and scanning electron microscopic studies of oviductal epithelium in Thai swamp buffalo (Bubalus bubalis) at the follicular and luteal phases. *Reprod Domest Anim* 2009; **44**: 450–455. [Medline] [CrossRef]
47. **Homburg R, Meltcer S, Rabinson J, Scharf S, Anteby EY, Orvieto R.** Is there a limit for the number of in vitro fertilization cycles for an individual patient? *Fertil Steril* 2009; **91**(Suppl): 1329–1331. [Medline] [CrossRef]
48. **Liang L, Xu B, Zhu G.** Effect of repeated gonadotropin stimulation on ovarian reserves and proliferation of ovarian surface epithelium in mice. *Front Med China* 2009; **3**: 220–226. [CrossRef]
49. **Kalthur G, Salian SR, Nair R, Mathew J, Adiga SK, Kalthur SG, Zeegers D, Hande MP.** Distribution pattern of cytoplasmic organelles, spindle integrity, oxidative stress, octamer-binding transcription factor 4 (Oct4) expression and developmental potential of oocytes following multiple superovulation. *Reprod Fertil Dev* 2016; **28**: 2027–2038. [Medline] [CrossRef]
50. **Paul LT, Atilan O, Tulay P.** The effect of repeated controlled ovarian stimulation cycles on the gamete and embryo development. *Zygote* 2019; **27**: 347–349. [Medline] [CrossRef]
51. **Chao HT, Lee SY, Lee HM, Liao TL, Wei YH, Kao SH.** Repeated ovarian stimulations induce oxidative damage and mitochondrial DNA mutations in mouse ovaries. *Ann N Y Acad Sci* 2005; **1042**: 148–156. [Medline] [CrossRef]
52. **Miyamoto K, Sato EF, Kasahara E, Jikumaru M, Hiramoto K, Tabata H, Katsuragi M, Odo S, Utsumi K, Inoue M.** Effect of oxidative stress during repeated ovulation on the structure and functions of the ovary, oocytes, and their mitochondria. *Free Radic Biol Med* 2010; **49**: 674–681. [Medline] [CrossRef]
53. **Xie JK, Wang Q, Zhang TT, Yin S, Zhang CL, Ge ZJ.** Repeated superovulation may af-

fect mitochondrial functions of cumulus cells in mice. *Sci Rep* 2016; **6**: 31368. [Medline] [CrossRef]

54. **Combelles CM, Albertini DF.** Assessment of oocyte quality following repeated gonadotropin stimulation in the mouse. *Biol Reprod* 2003; **68**: 812–821. [Medline] [CrossRef]
55. **Bondi AM, Gabrielli MG, Marchetti L, Materazzi G, Menghi G.** Cytomorphological changes in the rabbit oviductal epithelium after human chorionic gonadotropin treatment. *Histol Histopathol* 1997; **12**: 135–146. [Medline]
56. **Maillo V, Sánchez-Calabuig MJ, Lopera-Vasquez R, Hamdi M, Gutierrez-Adan A, Lonergan P, Rizos D.** Oviductal response to gametes and early embryos in mammals. *Reproduction* 2016; **152**: R127–R141. [Medline] [CrossRef]
57. **Leese HJ, Sturmey RG, Whitear S-L.** The Oviductal Environment and Early Embryo Development: A Question of Supply and Demand. *Biol Reprod* 2009; **81**: 57. [CrossRef]
58. **Schulte BA, Rao KP, Kreutner A, Thomopoulos GN, Spicer SS.** Histochemical examination of glycoconjugates of epithelial cells in the human fallopian tube. *Lab Invest* 1985; **52**: 207–219. [Medline]
59. **Leese HJ, Baumann CG, Brison DR, McEvoy TG, Sturmey RG.** Metabolism of the viable mammalian embryo: quietness revisited. *Mol Hum Reprod* 2008; **14**: 667–672. [Medline] [CrossRef]
60. **Li S, Winuthayanon W.** Oviduct: roles in fertilization and early embryo development. *J Endocrinol* 2017; **232**: R1–R26. [Medline] [CrossRef]
61. **Tamate K, Sengoku K, Ishikawa M.** The role of superoxide dismutase in the human ovary and fallopian tube. *J Obstet Gynaecol (Tokyo 1995)* 1995; **21**: 401–409. [Medline] [CrossRef]
62. **Agarwal A, Aponte-Mellado A, Premkumar BJ, Shaman A, Gupta S.** The effects of oxidative stress on female reproduction: a review. *Reprod Biol Endocrinol* 2012; **10**: 49. [Medline] [CrossRef]
63. **Fujii J, Iuchi Y, Okada F.** Fundamental roles of reactive oxygen species and protective mechanisms in the female reproductive system. *Reprod Biol Endocrinol* 2005; **3**: 43. [Medline] [CrossRef]
64. **Van Blerkom J.** Mitochondria in early mammalian development. *Semin Cell Dev Biol* 2009; **20**: 354–364. [Medline] [CrossRef]
65. **Hagiwara H.** Electron microscopic studies of ciliogenesis and ciliary abnormalities in human oviduct epithelium. *Ital J Anat Embryol* 1995; **100**(Suppl 1): 451–459. [Medline]
66. **Coan M, Rampioni Vinciguerra GL, Cesaratto L, Gardenal E, Bianchet R, Dassi E, Vecchione A, Baldassarre G, Spizzo R, Nicoloso MS.** Exploring the role of Fallopian ciliated cells in the pathogenesis of high-grade serous ovarian cancer. *Int J Mol Sci* 2018; **19**: 19. [Medline] [CrossRef]
67. **Ghosh A, Syed SM, Tanwar PS.** In vivo genetic cell lineage tracing reveals that oviductal secretory cells self-renew and give rise to ciliated cells. *Development* 2017; **144**: 3031–3041. [Medline] [CrossRef]
68. **Chang YH, Ding DC, Chu TY.** Estradiol and progesterone induced differentiation and increased stemness gene expression of human Fallopian tube epithelial cells. *J Cancer* 2019; **10**: 3028–3036. [Medline] [CrossRef]
69. **Ito S, Yamamoto Y, Kimura K.** Analysis of ciliogenesis process in the bovine oviduct based on immunohistochemical classification. *Mol Biol Rep* 2020; **47**: 1003–1012. [Medline] [CrossRef]
70. **Moussa M, Farouk SM.** Ovarian stimulation induces high expression of interleukin-1β and disrupts the histological features of the fallopian tube. *Turk J Vet Anim Sci* 2019; **43**: 186–196. [CrossRef]
71. **Nutu M, Weijdegård B, Thomas P, Thurin-Kjellberg A, Billig H, Larsson DG.** Distribution and hormonal regulation of membrane progesterone receptors beta and gamma in ciliated epithelial cells of mouse and human fallopian tubes. *Reprod Biol Endocrinol* 2009; **7**: 89. [Medline] [CrossRef]
72. **Okada A, Ohta Y, Inoue S, Hiroi H, Muramatsu M, Iguchi T.** Expression of estrogen, progesterone and androgen receptors in the oviduct of developing, cycling and preimplantation rats. *J Mol Endocrinol* 2003; **30**: 301–315. [Medline] [CrossRef]
73. **Wånggren K, Stavreus-Evers A, Olsson C, Andersson E, Gemzell-Danielsson K.** Regulation of muscular contractions in the human Fallopian tube through prostaglandins and progestagens. *Hum Reprod* 2008; **23**: 2359–2368. [Medline] [CrossRef]
74. **Gawronska B, Stepien A, Ziecik AJ.** Effect of estradiol and progesterone on oviductal LH-receptors and LH-dependent relaxation of the porcine oviduct. *Theriogenology* 2000; **53**: 659–672. [Medline] [CrossRef]
75. **Małysz-Cymborska I, Andronowska A.** Downregulation of LH and FSH receptors after hCG and eCG treatments in the porcine oviduct. *Domest Anim Endocrinol* 2016; **57**: 48–54. [Medline] [CrossRef]
76. **Sanner K, Conner P, Bergfeldt K, Dickman P, Sundfeldt K, Bergh T, Hagenfeldt K, Janson PO, Nilsson S, Persson I.** Ovarian epithelial neoplasia after hormonal infertility treatment: long-term follow-up of a historical cohort in Sweden. *Fertil Steril* 2009; **91**: 1152–1158. [Medline] [CrossRef]
77. **Lahav-Baratz S, Koifman M, Sabo E, Auslender R, Dirnfeld M.** p27 and its ubiquitin ligase Skp2 expression in endometrium of IVF patients with repeated hormonal stimulation. *Reprod Biomed Online* 2016; **32**: 308–315. [Medline] [CrossRef]
78. **Lacoste CR, Clemenson A, Lima S, Lecointre R, Peoc'h M, Chene G.** Tubo-ovarian dysplasia in relationship with ovulation induction in rats. *Fertil Steril* 2013; **99**: 1768–1773. [Medline] [CrossRef]
79. **See SHC, Behdad A, Maniar KP, Blanco LZ Jr.** Ovarian carcinosarcoma and concurrent serous tubal intraepithelial carcinoma with next-generation sequencing suggesting an origin from the Fallopian tube. *Int J Surg Pathol* 2019; **27**: 574–579. [Medline] [CrossRef]
80. **Soong TR, Howitt BE, Horowitz N, Nucci MR, Crum CP.** The fallopian tube, "precursor escape" and narrowing the knowledge gap to the origins of high-grade serous carcinoma. *Gynecol Oncol* 2019; **152**: 426–433. [Medline] [CrossRef]
81. **Cibula D, Widschwendter M, Zikan M, Dusek L.** Underlying mechanisms of ovarian cancer risk reduction after tubal ligation. *Acta Obstet Gynecol Scand* 2011; **90**: 559–563. [Medline] [CrossRef]
82. **Rice MS, Murphy MA, Vitonis AF, Cramer DW, Titus LJ, Tworoger SS, Terry KL.** Tubal ligation, hysterectomy and epithelial ovarian cancer in the New England Case-Control Study. *Int J Cancer* 2013; **133**: 2415–2421. [Medline] [CrossRef]